Shattered Pellet Injection experiments at JET in support of the ITER Disruption Mitigation System design

S. Jachmich[1], U. Kruezi[1], M. Lehnen[1], M. Baruzzo[2], L. R. Baylor[3], D. Carnevale[4], D. Craven[5], N. W. Eidietis[6], O. Ficker[7], T. E. Gebhart[3], S. Gerasimov[5], J. L. Herfindal[3], E. Hollmann[6], A. Huber[8], P. Lomas[5], J. Lovell[3], A. Manzanares[9], M. Maslov[5], J. Mlynar[7], G. Pautasso[10], C. Paz-Soldan[6], A. Peacock[5], L. Piron[11], V. Plyusnin[12], M. Reinke[3], C. Reux[13], F. Rimini[5], U. Sheikh[14], D. Shiraki[3], S. Silburn[5], R. Sweeney[15], J. Wilson[5] , P. Carvalho[12] and JET contributors[*]

[1] ITER Organization, Route de Vinon-sur-Verdon - CS 90 046, 13067 St Paul Lez Durance Cedex, France
[2] ENEA for EUROfusion, Via E. Fermi 45, 00044 Frascati (Roma), Italy
[3] Oak-Ridge National Laboratory, Oak Ridge, U.S.A.
[4] Dip. di Ing. Civile ed Informatica, Università di Roma "Tor Vergata", Italy
[5] CCFE, Abingdon, UK
[6] General Atomics, San Diego, U.S.A.
[7] Institute of Plasma Physics of the CAS, Prague, Czech Republic
[8] Forschungszentrum Jülich GmbH, Jülich, Germany
[9] Laboratorio Nacional de Fusion, CIEMAT, Madrid, Spain
[10] Max-Plank-Institut für Plasma Physik, Garching, Germany
[11] Consorzio RFX, Padova, Italy
[12] Instituto de Plasmas e Fusão Nuclear, Instituto Superior Tecnico, Universidade de Lisboa, Lisboa, Portugal
[13] CEA/IRFM, Saint-Paul-Lez-Durance, France
[14] Ecole Polytechnique Federale de Lausanne, Swiss Plasma Center, Lausanne, Switzerland
[15] Massachusetts Institute of Technology, Cambridge, USA
[*] see author list of 'Overview of JET results for optimizing ITER operation' by J. Mailloux *et al*, to be published in Nucl. Fus. Special Issue for 28th Fusion Energy Conference (2021).

Abstract

A series of experiments have been executed at JET to assess the efficacy of the newly installed Shattered Pellet Injection (SPI) system in mitigating the effects of disruptions. Issues, important for the ITER disruption mitigation system, such as thermal load mitigation, avoidance of runaway electron formation, radiation asymmetries during thermal quench mitigation, electromagnetic load control and runaway electron energy dissipation have been addressed over a large parameter range. The efficiency of the mitigation has been examined for the various SPI injection strategies. The paper summarises the results from these JET SPI experiments and discusses their implications for the ITER disruption mitigation scheme.

1. Introduction

An effective Disruption Mitigation System (DMS) that minimizes thermal excursions, mechanical forces and effects of Runaway Electrons (RE) is mandatory for the successful operation of ITER. The chosen ITER-DMS concept [1] is based on disruption mitigation through injection of shattered pellets, so-called SPI, which in ITER ensures a prompt delivery of the material to the plasma and promises a deeper deposition of the injected material compared to the commonly used Massive Gas Injection (MGI) valves. Pioneering work of this technique was done on DIII-D [2].

Despite of the huge advances in the design of the SPI system for the ITER-DMS [3], gaps in the understanding of the effectiveness of disruption mitigation with SPI still remain. To assist in addressing them, SPI experiments were needed to increase the confidence in the predictions

for ITER. For this purpose, the ITER Organization has established an international collaboration together with US DOE, UKAEA and EUROfusion to install a new SPI system at JET, which has been brought into operation during the most recent JET campaign. The JET SPI experiments, performed in the 2019-2020 campaigns on target plasmas with plasma currents of up to 3.0 MA and thermal energies up to 8MJ, are a key element to allow extrapolation to ITER in terms of size, plasma current and plasma energy. Moreover, the ITER-like wall is essential to address injections with low impurity content without being impacted by high carbon levels. These experiments serve as basis for the benchmarking of models that are required to predict the performance of the ITER-DMS. The key ITER needs to which the JET-SPI results contribute are on the thermal load mitigation, runaway electron avoidance through dilution cooling using deuterium (D) injection, control of the current quench (CQ) rate to keep the electromagnetic loads within limits, late injection into a current quench for radiating magnetic energy of a post thermal quench plasma and the dissipation of runaway electron energy to minimise the impacts on in-vessel components.

On ITER, hydrogen (H) is planned to be used for the propellant gas and main pellet material throughout all operational phases (including He and DT operation), raising the issue of a potential detrimental effect on the subsequent pulses due to dilution of the plasma main species with residual hydrogen. Tests in H-mode plasmas at JET with hydrogen injection revealed low levels of hydrogen retention in the following reference pulses, which support the design decision not to foresee deuterium for the ITER DMS. The experiments described in this paper use deuterium combined with high-Z gases as the mitigation processes are equivalent for use of hydrogen.

2. JET SPI system and related diagnostics

The JET Shattered Pellet Injection system consists of a three barrel pellet gun and is mounted on top of the machine (Figure 1). All barrels have different diameters and allow the desublimation of hydrogen, deuterium, neon, mixtures of these gases and argon. The injection capabilities are summarised in Table 1. The percentage of neon mixed into deuterium is defined as the ratio of neon atoms to the total number of atoms in the pellet, including a potential deuterium shell. The pellets can be dislodged and accelerated either by a pure gas puff or, in case of the two largest barrels, in combination with a mechanical punch. If used the punches are mounted in front of the propellant valves to utilize the gas impulse to accelerate the punch tip towards the pellet. When the punch stroke is at its maximum, the propellant gas can flow down the stem and through the punch tip to accelerate the dislodged pellet [4]. The pellets pass through a microwave cavity diagnostic [5], which allows the characterization of the pellet integrity, mass and velocity. After a travel time of ~7ms (B, 100%D w/o punch) to ~28ms (A, 100%Ne with punch), the pellets are shattered against an S-bend with an angle of 20°. The travel time of Ne/D-mixed pellets depends on the Ne-fraction, e.g. the travel of a 80%Ne/20%D B-pellet with punch is about 20ms. More details on the system can be found in [6]. The arrival time of the fragments in the plasma can be inferred from a fast camera observation, which can be equipped with different filters. The propellant gas, typically in the amount of 3.6×10^{21} D_2-molecules, is retarded by using a 1 m^3 expansion volume. The probability for a pellet being broken when it passes the microwave cavity is ~26% when no punch is used for the

dislodgment and 42% with the punch. One should note that additional breakage can occur prematurely before the shatter section is reached and might be possibly only identified from the fast camera observation at the injection point.

The radiation properties during the disruptions can be determined with two bolometer systems which are 78.5° and -155.5° toroidally away from the SPI. The radiated power at these locations is inferred from weighted sums.

Two external magnetic field coil pairs (called EFCC), originally designed to correct intrinsic error fields, can be used to superimpose an n=1 perturbation. By changing the polarity and amplitude of the two coil pairs, the main direction of the radial magnetic field perturbation can be varied.

The fragmentation of the pellets has been characterized in [7]. Pellets with higher velocities not only result in smaller fragments, but most importantly also in a dominant fraction of material being injected possibly as gas or liquid. For example, the mass accounted for in fragments of an A-pellet with 3.4%Ne+96.6%D at 575m/s is only 5% of the original pellet material, which increases to 26% at 450 m/s and in case of 90%Ne+10%D pellet at 250 m/s to 86%. The total mass accounted for in fragments is based on the assumption that the fragments are spheres with radii which are taken from the average of two orthogonal maximum lengths of each individual detectable fragment as determined by video analysis of fragment plume observations with a high speed camera. A high fraction of gas can significantly impact the particle assimilation and hence the disruption mitigation process. As seen in Figure 2, the current quench times for Ne/D mixed SPI-pellets injected into an H-mode plasma (I_p~2.5MA, W_{mag}~5.4MJ, W_{th}~3-4MJ) are shorter for slower pellets (blue squares/"with punch"), indicating a higher assimilation of Ne, resulting in a more resistive current quench plasma. Whether the change in assimilation is due to the larger amount of solid material or different fragment velocities will be subject of future SPI experiments at ASDEX-Upgrade [8]. For the experiments reported in this paper, the thermal energy, W_{th}, is taken from diamagnetic energy measurements and the magnetic energy, W_{mag}, is given by

$$W_{mag} = \frac{1}{2} L_p I_p^2 \quad , \tag{1}$$

where the total plasma inductance L_p can be approximated by

$$L_p = \mu_0 R_0 \left(1.8 * \frac{1-\frac{a}{R_0}}{1-\frac{a}{R_0}+0.4\kappa} + \frac{l_i}{2} \right) \tag{2}$$

with a as minor plasma radius, R_0 as major plasma radius, κ as plasma elongation and l_i as internal inductance.

3. Thermal load mitigation using mixtures of deuterium and neon

In ITER the mitigation of thermal loads during the thermal quench (TQ) must be effective to keep the conducted heat loads during major disruptions to below ~20 MJ. A sufficient quantity of assimilated Ne atoms can fulfil this task, but will also accelerate the current quench causing potentially the formation of runaway electrons (REs). A possible RE avoidance scheme is the combined injection of H and Ne. In [9] it has been reported that the radiated energy saturates for injected Ne quantities of more than ~10^{22} atoms for the disruptions shown in Figure 2.

However, from this analysis alone it is not possible to determine the amount of thermal energy being radiated. By varying the thermal energy for fixed magnetic energy, the fraction of energy radiated during the TQ can be inferred by extrapolating to thermal fractions of f_{th}=100%. Figure 3 shows such a scan for H-mode plasmas with 3MJ of magnetic energy and 0.3-1.5MJ of thermal energy using B-pellets with 80% Ne and 20% D ($2.4x10^{22}$ Ne, $6.1x10^{21}$ D). The energy coupled into the vessel and the poloidal field coils has been subtracted following the methodology described in [10]. The radiated energy fraction is shown for two different bolometric measurements, one using the vertical bolometer (blue circles) and one using the horizontal (red circles). For these two sets of data, the measured radiated energy was assumed to be axisymmetric. The limitation of this assumption will be evaluated further down in this paper. Since the vertical bolometer is closest to the shattered pellet injection location, the corresponding radiated energy fractions exceed the ones based on the horizontal bolometer providing an indication for the uncertainties in determining the radiated energy. Unlike reported in [11], a systematic decreasing trend of f_{rad} with f_{th} cannot be observed and the amount of radiated thermal energy varies from ~0% to 60~%. In fact, fast camera observations of the disrupting plasmas reveal a large helical structure during the TQ. Using radiation phantoms to match the individual line-of-sight measurements [12], the analysis can be improved, resulting in higher radiation efficiency [13]. However, in some cases the radiated fraction remains low. In this analysis a Gaussian toroidal distribution of the radiation around the injection location was assumed using the measured radiated powers as boundaries. With this assumption it was possible to derive a toroidal peaking factor TPF of about 2.2. The toroidal peaking factor is defined as $TPF = P_{rad,max}(\varphi)/< P_{rad}(\varphi) >$. One should note, that a possible existing n=1 mode, which is common in these disruptions, has not been taken into account.

4. Radiation asymmetries for SPI into plasmas with pre-existing n=1 mode

In order to determine the toroidal peaking factor of the radiation, either a good toroidal coverage with the bolometry diagnostic is required, or the toroidal distribution must be inferred from the change of the radiated power measured at a given toroidal location as a function of the location of the locked mode phase. At JET, external magnetic perturbation coils can be used to superimpose an n=1 perturbation field and to lock the phase in different toroidal locations. During the steady-state phase of an H-mode plasma (I_p=2.0MA, P_{aux}=14MW, W_{th}=2MJ, f_{th}~0.4), an additional n=1 field has been applied prior firing of the SPI. The coil current polarities and hence the prominent direction of the radial magnetic field perturbation have been varied on a shot-to-shot basis. The location of the locked mode phase has been derived from the magnetic measurements using a set of orthogonal saddle coils after substracting the vacuum pick-up fields. Two different types of pellets have been studied, both with the same Ne-amount (A, B=$2.4x10^{22}$ Ne-atoms) together with different amount of deuterium (A=$1.1x10^{23}$ D-atoms, B=$5.7x10^{21}$ D-atoms).

Figure 4 shows clearly the effect for a B-pellet injection on the radiation close to the SPI-location when the polarity of the perturbation field is changed such that the O-point locks almost opposite to the SPI ($\phi_{n=1} - \phi_{SPI}$=220°). The radiated power at the location of the vertical bolometer is strongly reduced, indicating a more symmetric radiation distribution. In order to

quantify the effect, the radiation asymmetry factor is determined during the TQ at the time when the radiation is maximum (as indicated by the dashed line).

For the six different directions of the radial magnetic perturbation field vector, which have been imposed in otherwise identical discharges, the radiation asymmetry is clearly impacted by the location of the n=1 O-point as illustrated in Figure 5. Despite the higher dilution with deuterium, the radiation asymmetries for the A-pellets are in fair agreement with the B-pellet scan. One should note that the current quench times of the B-pellet scan ($<t_{CQ}>$~22.1±0.5ms) and of the A-pellet scan ($<t_{CQ}>$~25.3±0.9ms) show no measurable variation with the O-point location. This is an important finding as it indicates that the particle assimilation is not impacted by whether the injection is done into an O-point or an X-point of an existing n=1 mode. The slightly longer current quench times for the lower Ne-fraction pellets are in agreement with the results presented in Section 6.

The toroidal peaking factor can be estimated by assuming a cosine-like radiation distribution $p_{dis}(\phi)$ driven by the n=1 mode [14] and a Gaussian-type toroidal distribution of the impurity density $n_i(\phi)$:

$$p_{dis}(\phi) = 1 + \Delta p \cos(\phi_{n=1} - \Delta\phi_{n=1} - \phi) \quad (3)$$

$$n_i(\phi) = n_{i,0} \exp\left(-(\phi - \phi_{inj})^2/\lambda_\phi^2\right) \quad (4)$$

with ϕ=[−π,π] as toroidal coordinate and ϕ_{inj} as toroidal location of the SPI. The width of the impurity density distribution and the amplitude of the variation by the mode, λ_ϕ and Δp, as well as the phase offset $\Delta\phi_{n=1}$ are free parameters that can be used to fit the model to the measured power asymmetries. The total radiation measured at a specific toroidal location is then given by

$$P_{rad}(\phi) = \langle P_{rad}(\phi)\rangle\, p_{dis}(\phi)\, n_i(\phi) \quad (5)$$

and the toroidal peaking factor TPF for a given location of the O-phase of an n=1 mode, ϕ_m, as

$$TPF(\phi_m) = P_{rad,max}(\phi_m)/\langle P_{rad}(\phi_m)\rangle\,. \quad (6)$$

Due to the limited dataset for the A-pellet scan, the model has been applied only to the 81% Ne injections and the resulting fit is indicated by the blue dashed line in Figure 5a. Using the derived parameters, the TPF can be calculated for all possible n=1 O-point locations (Figure 5b). For the worst case, when the O-point is close to the injection location, the TPF is maximum of about 1.7. Similar values have been reported for DIII-D in [2] and would allow for ITER poloidal peaking factors of the radiated power distribution up to 2.3 to keep the radiation induced heat flux factor below 4. Since the poloidal peaking factor might also be a function of the toroidal coordinate, the quoted limit is a lower bound. One should also note that the relevant wall heat flux peaking depends on the exact wall geometry.

5. Dilution cooling as runaway electron avoidance scheme

Dilution cooling is thought to aid the suppression of hot tail RE generation by repopulating hot electrons into lower energy ranges. The additional long pre-thermal quench duration would also be beneficial for increasing the plasma density for RE avoidance, reducing the thermal energy prior the occurrence of the TQ and, with the combination of these two effects, reducing the required amount of neon to achieve sufficient TQ radiation. Furthermore this could help relaxing the constraints on the maximum allowable jitter for the multiple SPI that is required

in ITER to achieve the target densities. This scheme has been tested on JET with pure deuterium injections into two different types of H-mode target plasma with thermal energies of ~4MJ and ~7-8MJ and magnetic energies respectively 16 MJ and 22 MJ. The resulting cooling duration, taken as the time lapse between arrival of the first fragments and the start of the TQ taken at the time of the plasma current minimum prior the current spike, is shown together with the data set from the conventional TQ mitigation scheme as described in Section 3 in Figure 6. Long pre-thermal quench times of up to ~70ms have been achieved for pure deuterium SPI. One should note that already the addition of a few percent of neon, close to the presently envisaged ITER range of 0.1% to 1% Ne-fraction, strongly reduces the cooling duration to well below 10ms. With increasing Ne-quantity the time to deliver and assimilate the fragments decreases further. The scatter for the 100% D_2-injection has been traced down to variation in the fragment delivery due to premature pellet breakage and different sequence of events. This is illustrated in Figure 7, where the temporal evolution for two pulses at W_{th}~8MJ with different cooling duration is shown. The times are plotted with respect to the fragment arrival time. By chance the pellets from barrel A were broken in a way that in pulse 96874 ~$1.4x10^{23}$ atoms were injected over ~7ms, whereas in pulse 96867 approximately $1.1x10^{23}$ atoms were delivered in two batches over ~12ms. In the first case, the large amount of ablated material leads to a fast increase in the radiation and soon a large helical structure forms followed by a fast rising n=1 mode. MHD simulations are needed to fully disentangle the causality of these events. The TQ occurs close to the level at which this event is expected to happen according to the scaling in [15]. In [16] it has been shown that this scaling is valid for a large set of SPI induced disruptions. The thermal energy is mainly lost through radiation on a very short timescale potentially causing high heat loads in ITER, whereas in 96867 about 2.8MJ are lost through transport on a characteristic timescale of ~150ms and ~2.0MJ are radiated prior the termination. Provided the convected and conducted energy loss in this phase would occur in ITER on comparable time scales, such a mechanism would relax the requirements on the subsequent TQ mitigation significantly.

Pulse 96867, which mimics to some extent a multiple injection, disrupts differently than 96874. The initial injected fragments cause only a modest rise of radiation and the typical helical structure usually observed in the fast camera images is not seen. In fact, the second batch is fully assimilated until the last fragments do not penetrate further into the plasma and are repelled outwards in the ion diamagnetic direction. This effect might be due to friction or a rocket effect as described in [17]. It is worthwhile noting that at this time the laser signal of the interferometer is lost due to refraction, which is typically a sign of high, peaked core density, and also initiates a plasma rampdown. As a consequence, a MARFE starts to develop after ~47ms, leading to a n=1 mode. Although the mode amplitude remains below the expected level for triggering the TQ, the locked mode triggers the massive gas injection valve (MGI) for disruption heat load protection. Unlike in the pulse with the short cooling duration, about 65% of thermal energy has been dissipated before the phase was terminated by the MGI.

The present examples of this injection scheme demonstrate the potential advantages of extended cooling durations, but also show that the fragment injection must be carefully tailored when using multiple SPIs. More experimental efforts are required to gain more insights into

the optimum deuterium fragment injection (multiple pellets), identification of the cause of the MHD mode onset and growth rates and the required final injection prior the start of the TQ.

6. Current quench control

To keep the electromagnetic forces on the ITER blanket modules within the design limits, the CQ times must remain within a range of 50-150 ms [18]. At JET, the sensitivity of the current quench has been tested by injecting different neon amount and fraction of Ne/D mixed SPI. Against expectation, the current quench duration is found not to depend on the total injected quantity but on the neon fraction, as seen in Figure 8. This is due to the TQ being triggered before all injected fragments are fully assimilated, i.e. the current quench is initiated at the same Ne/D quantity. For neon fractions above ~25% the current quench times can be controlled within the corresponding target range for ITER for the range of tested plasma currents (circle and diamond symbols).

In [19] examples were presented in which during the current quench fragments have been observed over a duration of 10ms and 1.5m into the plasma core. The rather long spatial spread can be explained with a velocity dispersion of ~40%, which has been confirmed in lab experiments [7]. These camera images also illustrate that a large fraction of fragments are still not ablated after the TQ.

ITER requires very high reliability of heat and electro-magnetic force mitigation during the current quenches of high current plasmas. To this end, the ITER DMS must also be efficient when triggered upon the detection of the TQ. Therefore, it is important to understand how efficient SPI is for injections into a low temperature, post thermal quench plasma. At JET, the effectiveness of SPI on post-disruptive plasmas, has been examined by inducing a density limit disruption using a large MGI of ~2×10^{21} molecules of pure deuterium into an ohmic plasma (W_{th}~0.9MJ, W_{mag}~10MJ), resulting in a long current quench time of ~58ms (blue curve in Figure 9a), typical for unmitigated disruptions in JET with the ITER-like wall [20]. In a subsequent pulse, SPI-barrel C with 60%Ne+40%D (3.3×10^{21} Ne, 1.8×10^{21} D-atoms) has been triggered such that the fragments arrive after 12ms (c.f. red arrow) into the current quench. The CQ is accelerated as indicated by the change of the plasma current slope (red curve) resulting in a current quench duration of ~23.8ms, similar to an SPI-induced disruption using the same neon and deuterium quantity (green curve). As indicated by the measured radiated power (c.f. red curves in figure 9b), this injection into the current quench is still effective in increasing the plasma radiation and hence dissipating the magnetic energy. The radiation has more than doubled and the energy conducted to the first wall was reduced from ~4.8MJ to ~2.8MJ. This suggests that despite the late injection, about 2/3 of the energy could still be radiated compared to a pre-TQ injection, which reduces the conducted energy to 1.8MJ. Here, the radiated energy was estimated conservatively assuming axisymmetry of the radiation and using the measured radiated power from the horizontal bolometer.

7. Runaway electron impact mitigation

In the case of accidental runaway electron generation in ITER, a scheme to dissipate their energy prior to the loss of the RE-beam must be in place. Injections of both pure argon and neon shards into a fully developed RE-beam in JET were the prime candidates to reduce the RE current based on theoretical work [21]. In order to test the viability of high-Z SPI injections, a scenario has been developed where a RE-beam is generated by a pure argon-MGI, with an amount twice the deuterium atom inventory of the pre-disruptive plasma, into a limiter plasma with low elongation and vertically controlled using an improved stabilization algorithm to achieve long RE beam durations [22]. For pre-disruptive plasma currents of 1.5 MA, RE-beams of ~700kA for up to 1 sec have been achieved with this method. At 350ms after the RE beam was formed, argon or neon were injected using the two largest barrels A and B. The collisions between REs and the high-Z atoms causes a decay in current and destabilises the RE beam vertically, leading to its scraping-off and shrinking and eventually to the destabilisation of MHD provoking a complete loss of the remaining REs. Figure 10 shows the termination phase of these pulses. The RE-beam can be successfully shortened and it is found that larger amounts of injected material (red and green time traces compared to magenta and black) lead to faster current drop and vertical movement. The final collapse occurs at smaller RE currents than in the unmitigated case. However, IR-camera data revealed that the heat fluxes to the inner wall during this final collapse are equivalent to those of unmitigated RE beams with the same current at the collapse [23]. Despite its higher atomic number, argon leads to similar beam termination as neon, which appears to contradict theoretical predictions [22], but can be attributed to the much lower density of Ar pellets and therefore less injected material (c.f. Table 1). Based on these results, ITER has decided for reasons of gas processing and cryogenic services to discard pure argon SPI as a possible mitigation scheme for the RE impact. Furthermore, these results also show that high-Z injection is questionable as a mitigation scheme for ITER, since in ITER the vertical movement is a direct function of the RE current [24].

An alternative to using high-Z, is the concept of low-Z, H or D, injection as studied previously at DIII-D [25, 26]. Following an injection of a 100% D barrel-A SPI (Figure 11), the loop voltage decreases, which is an indication of impurity purging, and the neutron and hard x-ray (HXR) rates drop. Since the plasma has low resistance and a higher plasma current is requested, the plasma current rises again until the final loss occurs, which is similar to an ohmic current quench. However, this phase is accompanied by the absence of a re-avalanching of REs, probably due to the short free mean path and, combined with a strong kink mode, possibly resulting in a larger wetted area [23, 27], ends in a benign termination. For these cases no heat flux at the final loss could be determined, since the IR data remained below the sensitivity threshold [23]. In conclusion, no measureable energy deposition during the final MHD event takes place. The applicability of this scheme to ITER is discussed in more detail in [27].

8. Summary and outlook

In JET with the ITER-like wall, it has been demonstrated that disruptive thermal loads can be effectively reduced through a combined Ne/D injection using shattered pellet injection. Due to large radiation asymmetries and the unknown material assimilation, modelling is required to quantify the efficiency. For this purpose modelling activities are ongoing within the domestic

programmes to assist the data interpretation. In addition, the ITER DMS Task Force (TF) has launched a substantial modelling programme to provide projections to ITER [28]. The conditions in which the experiments were performed significantly increased the parameter range of the available data for SPI mitigated disruptions. The observed toroidal peaking factors of the radiation are not of concern. However, more spatial resolved bolometer measurements, IR measurements and modelling using synthetic diagnostics are needed to conclude whether the total peaking remains below the values which would lead to for flash melting of the ITER beryllium first wall panels at the highest stored energies. The concept of dilution cooling to achieve long pre-thermal quench phases potentially reduces the chances of hot tail RE seeds and has offered the possibility of multiple pellet injection to raise the density and to reduce the thermal energy prior the triggering of the TQ. Since the scheme is sensitive to the fragment delivery, more experiments are needed to make this a robust mitigation strategy and to determine the required neon amount for the final mitigation of the disruption. Injections of high-Z fragments into an existing RE beam successfully shorten its duration, but the deposited energy at its final loss is governed by the amount current dissipation driven by the vertical movement. On the contrary, a low-Z shattered pellet injection into an existing RE beam not only helps to reduce the chances of high energy deposition at the final termination, but also eases the constraints on the overall DMS injection sequence by avoiding the risk of too early injections of high-Z material into an ongoing disruption. In order to scrutinise this method further, modelling using 3D-MHD codes such as JOREK [29] are being performed as part of the activities coordinated by the theory and modelling group of the ITER DMS TF [28]. The JET shattered pellet injection experiments, together with SPI studies carried out on other devices, have strengthened the decision to use this technology as the baseline for the ITER DMS.

Acknowledgements

The ITER DMS Task Force receives funding through the ITER Organization. This work has been carried out within the framework of the EUROfusion Consortium and has received funding from the Euratom research and training programme 2014-2018 and 2019-2020 under grant agreement No 633053. The views and opinions expressed herein do not necessarily reflect those of the ITER Organization or of the European Commission.

References

[1] Lehnen M., Campbell D., Hu D., Snipes J., Sweeney R., Maruyama S., Luce T., Kruezi U., R&D for reliable disruption mitigation in ITER. Preprint: 2018 IAEA Fusion Energy Conference, Gandhinagar (India), EX/P7-12.

[2] Commaux N. *et al*, Nucl. Fus. 56, 2016, 046007.

[3] Luce T., Kruezi U., Lehnen M., Jachmich S., De Bock M., Ellwood G., Progress on the ITER DMS design and integration. Preprint: 2020 IAEA Fusion Energy Conference, Nice, TECH/1-4Ra.

[4] Baylor L. *et al*, Nucl. Fus. 59, 2019, 066008.

[5] Sørensen H. *et al*, Rev. Sci. Instr. 61, 1990, 3464.

[6] Baylor L. *et al*, Design and Performance of Shattered Pellet Injection Systems for JET and KSTAR Disruption Mitigation Research in Support of ITER. Preprint: 2020 IAEA Fusion Energy Conference, Nice, TECH/1-4Rb.

[7] Gebhart T. *et al*, Fus. Sci. Tech. 77, 2021, 33.

[8] Papp G. *et al*, IAEA Technical Meeting on Disruptions, ITER, 2020.

[9] Sheikh U., Shiraki D., Sweeney R., Jachmich S., Joffrin E., Lehnen M., Lovell J., JET Contributors, Disruption Thermal Load Mitigation with JET SPI. Preprint: 2020 IAEA Fusion Energy Conference, Nice, EX/P3-7.

[10] Lehnen M. *et al*, Nucl. Fus. 53, 2013, 093007.

[11] Jachmich S. *et al*, 22nd PSI-conference, 2016.

[12] Lovell J. *et al*, Rev.Sci.Instr. 92, 2021, 023502.

[13] Sweeney R. *et al*, 62nd APS DPP meeting, 2020.

[14] Lehnen M. *et al*, Nucl. Fus. 55, 2015, 123027.

[15] De Vries P. *et al*, Nucl. Fus. 56, 2016, 026007.

[16] Shiraki D. *et al*, DIII-D and International Research towards Extrapolating Shattered Pellet Injection Performance to ITER. Preprint: 2020 IAEA Fusion Energy Conference, Nice, EX/5-2Ra.

[17] Senichenkov I., Rozhansky V., Gusakov P., 34th EPS Conference, ECA 31F, 2007, P-4.094.

[18] Sugihara M. *et al*, Disruption Impacts and their Mitigation Target Values. 2012 Proc 24th Int. Conf. on Fusion Energy (San Diego, 2012), ITR/P1-14 http://www-naweb.iaea.org/napc/physics/FEC/FEC2012/index.htm.

[19] Gerasimov S. *et al*, IAEA Technical Meeting on Disruptions, ITER, 2020.

[20] Lehnen M. *et al*, Nucl. Fus. 53, 2013, 093007.

[21] Martin-Solis J.R. *et al*, Nucl. Fus. 57, 2017, 066025.

[22] Carnevale D. *et al*, Plasm. Phys. Contr. Fus. 61, 2019, 014036.

[23] Reux C. *et al*, Phys. Rev. Letters 126, 2021 175001.

[24] Kiramov D.I., Beizman B.N., Phys. Plasm. 24, 2017, 100702.

[25] Paz-Soldan C. *et al*, Plasm. Phys. Contr. Fus. 61, 2019, 054001.

[26] Hollmann E. *et al*, Phys. Plasm. 27, 2020, 042515.

[27] Paz-Soldan C. *et al*, A novel path to runaway electron mitigation via deuterium injection and current-driven kink instability. Preprint: 2020 IAEA Fusion Energy Conference, Nice, EX/5-2Rb.

[28] Nardon E. *et al*, Theory and Modelling activities in support of the ITER Disruption Mitigation System. Preprint: 2020 IAEA Fusion Energy Conference, Nice, TH/6-1.

[29] Bandaru V. *et al*, Plasm. Phys. Contr. Fus. 63, 2021, 035024.

Tables

Barrel	Diameter [mm]	Length [mm]	H [atoms]	D [atoms]	Ne [atoms]	Ar [atoms]
A	12.5	19.3	$1.2\ 10^{23}$	$1.4\ 10^{23}$	$1.0\ 10^{23}$	$5.8\ 10^{22}$
B	8.1	13.0	$3.4\ 10^{22}$	$4.0\ 10^{22}$	$2.9\ 10^{22}$	$1.6\ 10^{22}$
C	4.6	6.4	$5.4\ 10^{21}$	$6.3\ 10^{21}$	$4.5\ 10^{21}$	N/A

Table 1: Injection parameters of the JET-SPI.

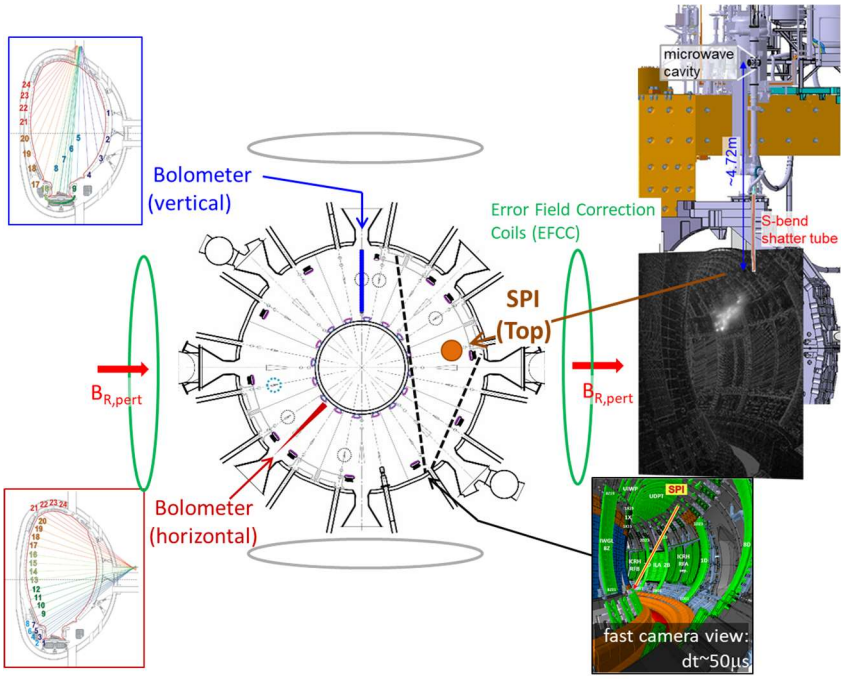

Figure 1: Toroidal cross-section of the JET tokamak, in the upper right the SPI on top of the machine and fragment ablation seen by a fast tangential camera view, two bolometer systems with 24 channels each and their respective mainly vertical and mainly horizontal line-of-sights. In addition the two Error Field Correction Coil pairs are indicated (green and grey).

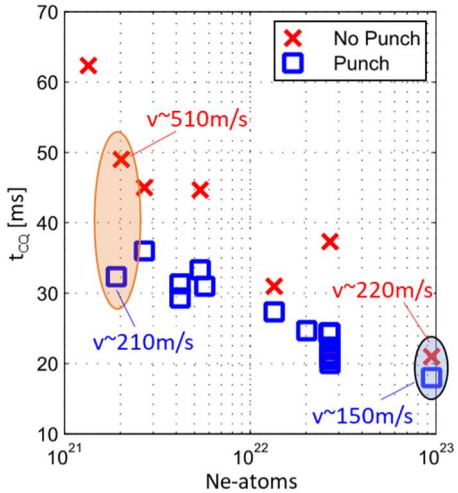

Figure 2: Current quench time for Ne/D-mixed pellets from barrels A and B without (red crosses) and with punch (blue squares). For two pellet pairs the velocities are indicated.

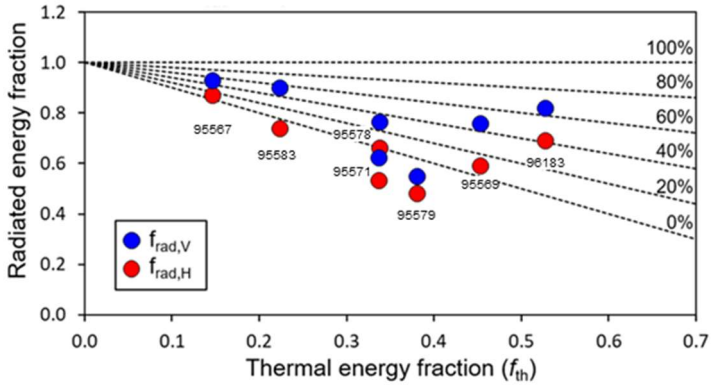

Figure 3: Radiated energy fraction determined using the radiated energy measured by the vertical (blue) and horizontal (red) bolometer. The dashed lines indicate the fraction of radiated thermal energy.

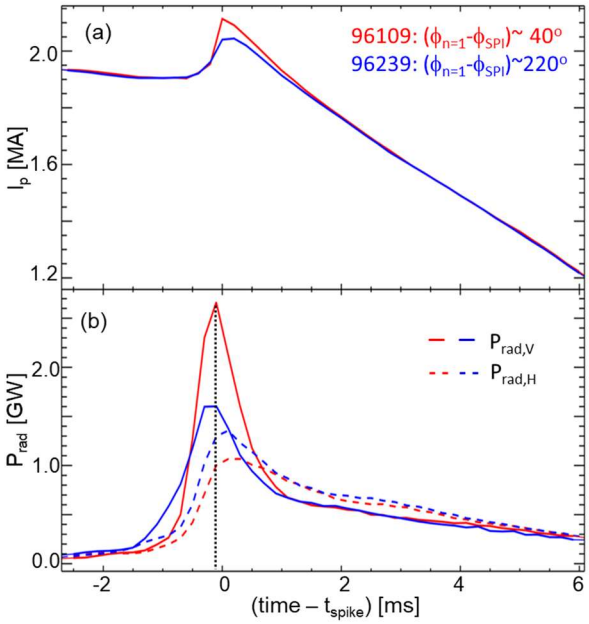

Figure 4: Time traces of (a) plasma current and (b) radiated power measured by the vertical (solid lines) and horizontal (dashed lines) bolometer for two different n=1 locked mode phases. The black vertical dashed line indicates the time when the radiation asymmetry factor is determined.

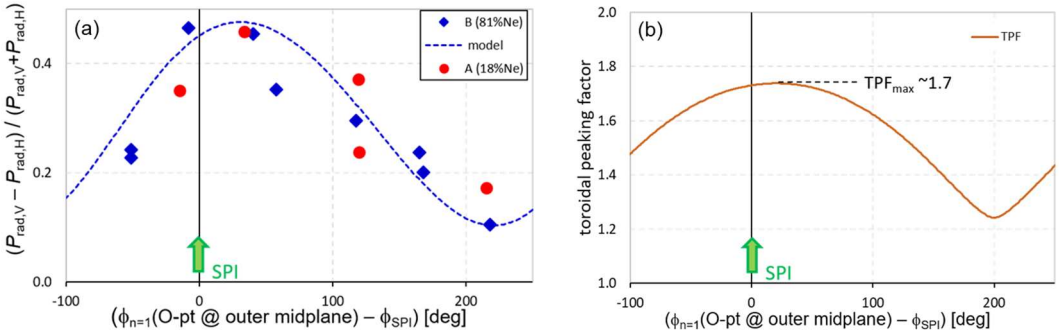

Figure 5: (a) Radiation asymmetry factor taken at the time of the maximum P_{rad}-peak as a function of the toroidal n=1 O-point location with respect to the SPI location for two data sets using different pellet types. The dashed line corresponds to the model fit using the data from the pellet B data set only. The fit parameters are λ_n=135°, $\triangle p$=0.22, $\triangle\phi_{n=1}$=-20°. (b) Resulting toroidal peaking factor as function of n=1 O-point location.

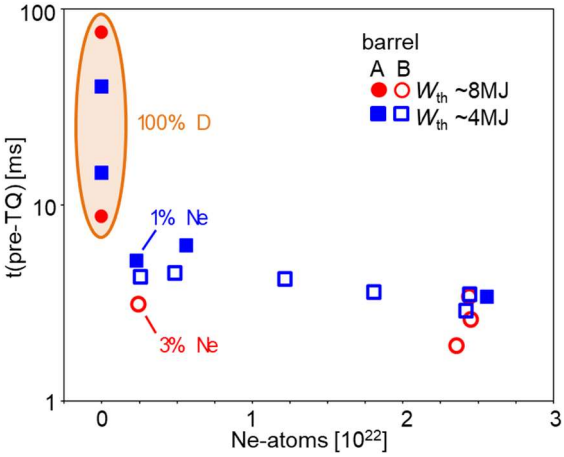

Figure 6: Cooling duration $t_{pre\text{-}TQ}$ for two different target plasmas (red and blue symbols) and two different sizes of Ne/D-mixed pellets (A=closed and B=open symbols) as function of injected Ne-atoms.

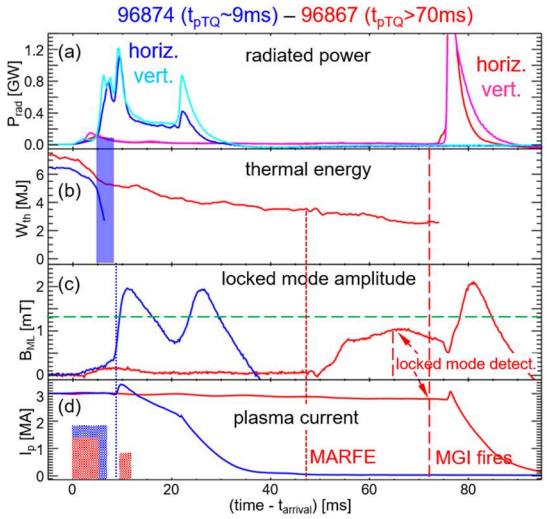

Figure 7: Comparison of two D-SPIs resulting in different pre-TQ times with (a) radiated power, (b) thermal energy, (c) n=1 locked mode amplitude with level at which TQ is predicted as in [14] (green dashed line) and (d) plasma current. The rectangles in (d) indicate the amount of material arriving in the plasma.

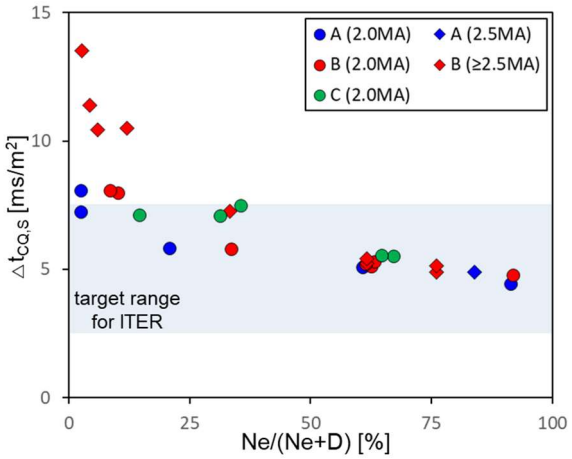

Figure 8: Current quench times extrapolated from 80% to 20% I_p drop duration normalised to the plasma surface as function of neon fraction. The colour code refers to different pellet sizes and the symbols to different ranges of pre-disruptive plasma current. The grey area indicates the corresponding target range for ITER current quench times.

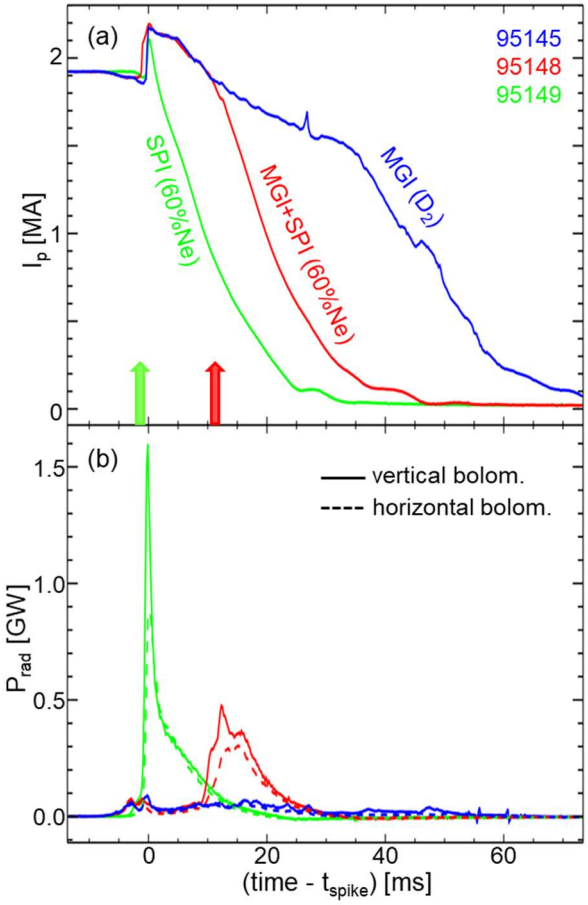

Figure 9: Time traces of (a) plasma current following pure-D_2 MGI-injection (blue), then mitigated with SPI with 60%Ne/40%D (red) and pure SPI with same composition (green). The radiated power measured by the vertical (solid lines) and horizontal (dashed lines) are shown in box (b). The arrows indicate the approximate arrival time of the fragments.

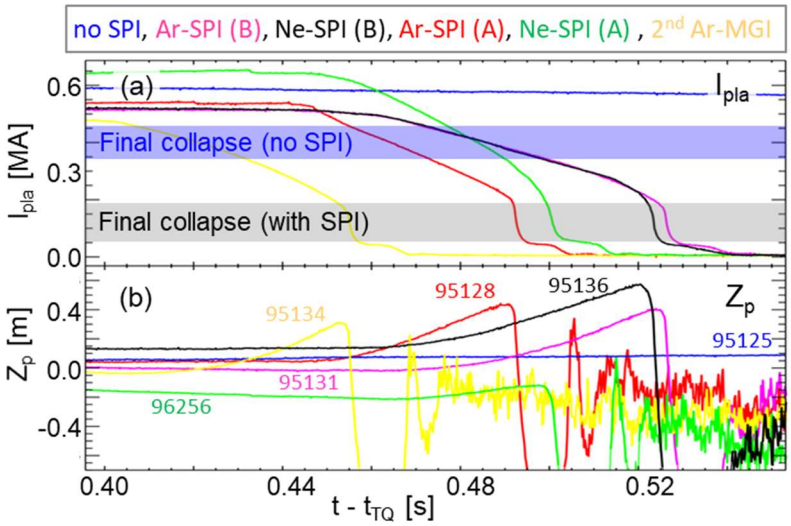

Figure 10: Time traces with respect to thermal quench time of (a) runaway current and (b) vertical position of plasma centroid. Colour codes correspond to the different injection attempts to dissipate the energy. The blue and grey boxes indicate approximately the I_p when the RE-beam is lost into the wall respectively without or with mitigation attempt.

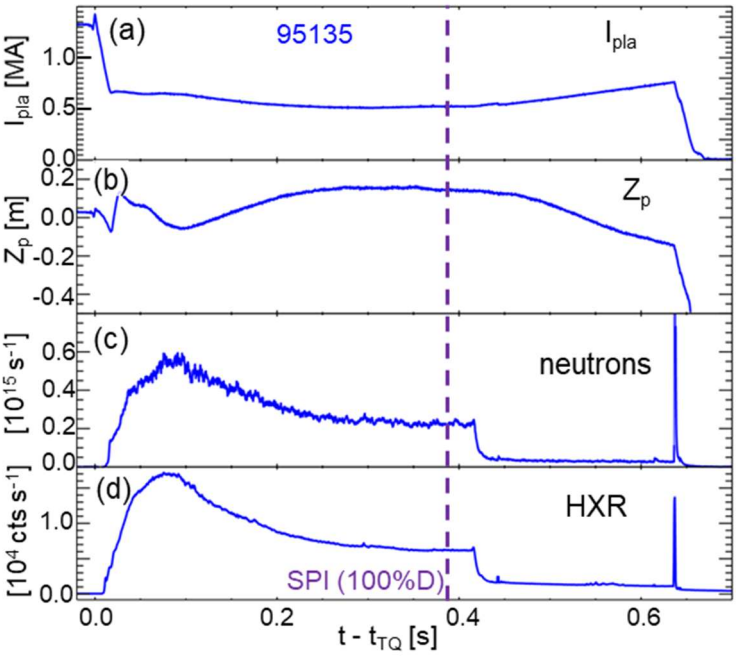

Figure 11: Time traces with respect to thermal quench time of (a) plasma current, (b) vertical position of plasma centroid, (c) neutron rate and (d) hard x-ray count rate. The vertical dashed line marks the time of the pure deuterium SPI.